A comparative study of triaxial and uniaxial magnetic shields made out of YBCO coated conductors

L Wéra[1], J-F Fagnard[1], G A Levin[2], B Vanderheyden[1] and P Vanderbemden[1]

[1]*University of Liège, SUPRATECS research group, Department of Electrical Engineering and Computer Science (B28), B-4000 Liège, Belgium*

[2]*Florida Institute of Technology, Department of Physics and Space Sciences, Melbourne, FL, USA*

E-mail: laurent.wera@ulg.ac.be

8 June 2015

Abstract

Persistent current loops of arbitrary size can be made from currently manufactured RE123 coated conductors. Our previous work has shown that an assembly of such loops is able to shield effectively quasi static axial magnetic field due to the absence of resistive joint. The shielding effectiveness depends on the aspect ratio and the number of layers. In the present work we study experimentally the detailed magnetic response of two different configurations of the magnetic shields for various orientations of the applied field. Using a 3-axis Hall probe we determine the amplitude of magnetic field generated by the induced persistent currents and its direction with respect to the applied field. The effectiveness of the uniaxial shield decreases strongly when the applied field is not collinear with its axis. In the triaxial (Polywell type) structure comprised of three pairs of coils whose axes are mutually orthogonal, the field attenuation is shown to be only weakly dependent on the direction of the magnetic field. We discuss the properties of the triaxial shield and the ways to improve its screening performance.

1. Introduction

Several scientific devices, e.g. cryogenics current comparators [1], DC current transformers [2], or superconducting quantum interference devices [3, 4], need a low magnetic field environment and must be shielded. High-field superconducting magnets used e.g. in MRI [5] or other applications [6, 7], need to be shielded to reduce their magnetic footprint. For low frequencies, a ferromagnetic material, such as permalloy or mu-metal, can be used [8]. In cryogenic applications, shielding with superconducting materials is found to be more effective than conventional ferromagnets and can be implemented easily since the cooling system is directly available. In particular, high temperature superconductors (HTS) hollow cylinders, made of $Bi_2Sr_2Ca_2Cu_3O_{10}$ (Bi-2223) [9, 10], $Bi_2Sr_2CaCu_2O_8$ (Bi-2212) [11, 12], $YBa_2Cu_3O_7$ (YBCO) [13, 14] or MgB_2 [15, 16], have already demonstrated their shielding abilities. Hybrid ferromagnetic/superconductor structures can also be used as DC magnetic shields [17, 18]. Moreover, it is also possible to use a combination of a Bi-2223 bulk cylinder and YBCO tape rings to improve the shielding performances of AC magnetic fields [19].

Additionally to superconducting coils [20, 21] or fault current limiters [22-24], YBCO 2G coated conductor sections can be used to build an efficient passive magnetic screen (throughout the paper we will use the terms shield and screen interchangeably as is a common practice in literature on this subject) that is able to shield axial and DC magnetic fields [25, 26]. The screen is built by milling the coated conductor sections and by placing them around a cylindrical support in order to form a joint-free superconducting loop where persistent currents can flow and provide a strong attenuation of a magnetic field. A schematic illustration of such a structure made of stacked 2G coated conductors is shown in figure 1. Compared to the bulk high temperature superconductors (HTS), the main advantages of using such structures as magnetic shields are: (i) the higher current density, (ii) the lower weight, and (iii) the scalability of the structure, leading to higher shielded volumes. Compared to other shields made out of coated conductors [25, 27], such a structure allows the persistent current to circulate around the screened volume without a superconducting joint.

In our earlier work (ref. [26]) we have studied how DC magnetic shielding performances can be improved by modifying geometrical parameters of the shield, i.e. the number of coated conductor sections stacked along the axis and the number of layers. The shielding performances are generally characterized by two parameters: (i) the shielding factor *SF*, defined as the ratio between the applied magnetic induction $B_{app} = \mu_0 H_{app}$ and the magnetic induction measured inside the structure B_{in} ($SF = B_{app}/B_{in}$) and (ii) the threshold induction B_{lim}, defined for a given value of the shielding factor. We have shown experimentally that the shielding factor *SF* and the threshold induction B_{lim} at the centre of the shield both increase with the aspect ratio (defined as the ratio between the mean height of the shield and the diameter of the supporting cylinder), while the threshold induction increases with the number of layers.

Until now, such passive shields made of stacked loops of coated conductors have only been characterized for an axial shielding, i.e. when the magnetic field is applied along the main axis of the shield. This corresponds to the configuration where the shield is the most efficient since induced shielding currents naturally flow in each of the closed loops of the stack. For practical applications however, it is important to determine how a passive magnetic shield reacts to magnetic field of *arbitrary* direction.

The aim of the present work is therefore twofold. First, we characterize experimentally a shield made out of one stack of loops (a uniaxial structure) for various orientations of the applied magnetic field with respect to the main axis of the shield. Second, we study experimentally the DC field attenuation properties of a structure that would be able to react to a DC magnetic field of arbitrary orientation. Such a structure is obtained by placing pairs of coils made out of coated conductors along the three orthogonal axes. This triaxial configuration is similar to the Polywell magnetic trap for plasma confinement [28].

The effectiveness of the triaxial screen has been measured for three different orientations of the applied magnetic field: a) the field is parallel to one of the axes; b) the field is perpendicular to one of the axes and makes an angle of 45° with two others, and c) the field is applied at equal angle to all three axes. Finally, we discuss the ways to improve the performance of the triaxial shield through the increased number of the sections of coated conductors and/or the increased critical current.

2. Experiment

2.1. Uniaxial structure

To make the magnetic screens studied in this paper we have used closed loops made out of YBCO 2G coated conductors using the procedure described in [25, 26, 29]. Figure 1 shows the main geometrical parameters of the uniaxial screen such as the height *h* and the diameter $D = 2R$ of the supporting cylinder upon which the superconducting loops are stacked. Unlike the superconducting bulk tubes, such a shield does not have the axial symmetry.

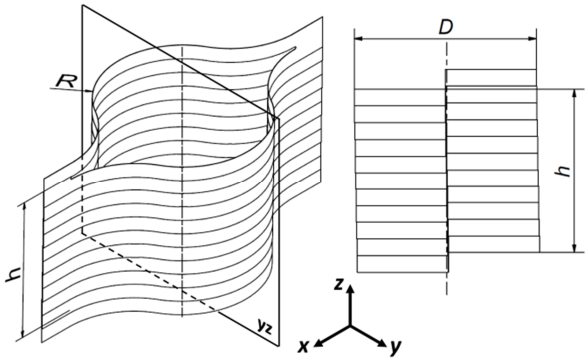

Figure 1. A sketch of a shield comprised of several coated conductor sections. The main geometrical parameters of a screen are: the diameter $D = 6$ cm and height *h* which is determined by the number of coated conductor sections. The Aspect Ratio is defined as $AR = h/D$. Note that the *x*-axis is chosen along the greater size of the loop, passing through the sharp tips of the loops.

In this work we characterize the shielding performances of a stack of 14 tapes (the uniaxial shield). Table 1 summarizes its characteristics. It should be noted that the coated conductor sections have somewhat varying critical current values [26]. The critical current density was found experimentally to range between 23.25 10^5 A/cm² and 27.25 10^5 A/cm², with an average value of 25.25 10^5 A/cm². In order to have a smooth and symmetrical distribution of the current density in the shield, we have placed the sections with the highest-I_C in the centre of the stack and the lowest I_C sections near the ends of the stack.

Table 1. Characteristics of the shield.

Number of tapes along the shield axis	N = 14
Height of the shield	h = 70.5 mm
Inner diameter	D = 60 mm
Aspect ratio	$AR = h/D$ = 1.175

Since there is no axial symmetry (figure 1), we consider two configurations for the orientation of the applied magnetic field with respect to the structure. Figure 2(a) shows a schematic illustration of the first configuration in which the main axis z of the shield rotates by a polar angle θ with respect to the direction C of the applied magnetic field H_{app}. The direction of the applied magnetic field is always parallel to the plane of symmetry yz. The angle θ ranges from 0° to 90° so that θ = 0° corresponds to the axial orientation and θ = 90° corresponds to the transverse orientation. Figure 2(b) shows a schematic illustration of the second configuration in which the main axis of the stack z remains perpendicular to the direction C of the applied magnetic field and the stack is rotated about its main axis z by the azimuthal angle α. The angle α ranges from 0° to 90°. Note that both configurations are equivalent for θ = 90° and α = 0°.

The shield is cooled down at 77 K and is subjected to a uniform quasi static (DC) magnetic field slowly ramped up at a constant rate of 1 mT/s. The magnetic field is generated by a copper source coil of 450 mm height and 200 mm diameter fed with a *Delta Elektronika*® (70 V-22 A) power supply. For both configurations, an *AREPOC*® (*axis 3*) 3-axis cryogenic Hall probe measures the three components of the local magnetic induction along the z-axis of the shield and at an elevation that corresponds to the centre of the shield. In the first configuration, the Hall probe rotates with the shield whereas in the second one, the Hall probe is fixed.

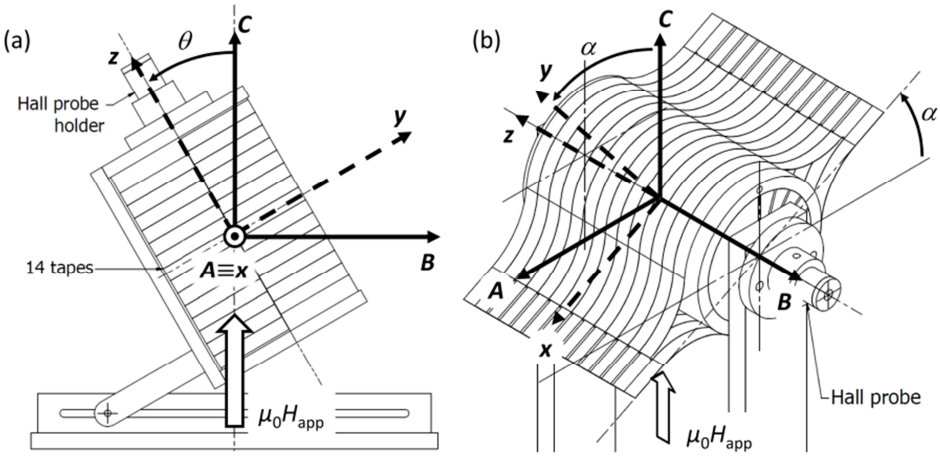

Figure 2. (a) Configuration #1. The axes (*A*, *B*, *C*) indicate the orientation of the applied field. The axes (*x*, *y*, *z*) (dashed lines) are associated with the shield and the Hall probe. (b) Configuration #2. The notations of the axes are the same as in 2(a). Here the Hall probe is not rotated with the shield. Note that the angle $\alpha = 0^\circ$ corresponds to the applied field directed along the shortest length of the loop. Angle $\alpha = 90^\circ$ corresponds to the applied directed along the sharp tips of the loops.

2.2. Triaxial structure

To build the triaxial screen, three cylindrical supports (6 cm diameter each) are assembled along the three orthogonal axes (figure 3). Six "coils", each consisting of two sections of double layered coated conductors (two tapes are superimposed to form a single double layered tape), were attached to the support structure forming a Polywell type [28] arrangement. The shielded interior of the screen has the volume approximately 6^3 cm^3. Note, that unlike the uniaxial shield, the triaxial one allows ready access to the content of the screened volume from all three directions. The stack height is optimized to allow the structure to be inserted into the liquid nitrogen container (about 15 cm diameter), regardless its orientation. Table 2 summarizes the geometric parameters of an individual stack. The highest and lowest I_C sections were distributed such as to make all six coils approximately equivalent.

Table 2. Geometric parameters of an individual stack.

Number of sections along each axis	$N = 4$
Number of layers	$m = 2$
Stack height	$h = 5.5$ mm
Inner radius	$R = 30$ mm
Aspect Ratio	$AR = h/(2R) = 0.0917$
Average critical current of a tape	$I_C = 125$ A

The DC magnetic field attenuation properties of the structures were characterized for three orientations of the applied magnetic field. In the first orientation (figure 3(a)), the *z*-axis of the shield is parallel to the direction of the applied magnetic field. In the second orientation (figure 3(b)), the structure is rotated about the *x*-axis so that *y* and *z* axes make an angle of 45° with respect to the direction of the applied magnetic field. In the third orientation (figure 3(c)), all three axes of the shield make the same angle ($\arccos\left(1/\sqrt{3}\right) \approx 54.74°$) relative to the applied field.

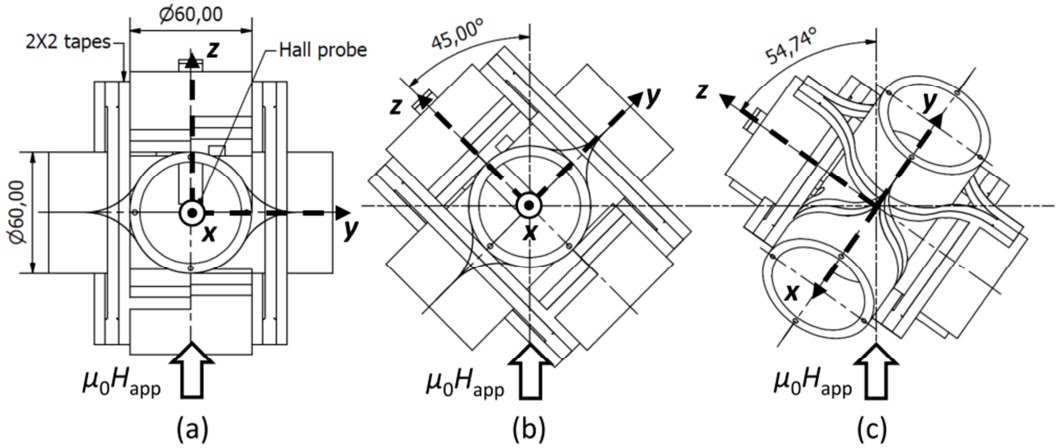

Figure 3. Schematic illustration of a 3-axis structure with different orientations with respect to the direction of the applied magnetic field: (a) H_{app} applied along *z*-axis, (b) 45° degrees angle between the direction of H_{app} and two of the axes (*z* and *y*), and (c) the equal angle of 54.74° ($\arccos\left(1/\sqrt{3}\right)$) between the direction of H_{app} and each of the axes.

For all orientations, the structure is cooled down at 77 K and is subjected to a uniform quasi static magnetic field slowly ramped up to 50 mT with a constant sweep rate of 1 mT/s. A 3-axis Hall probe measures the three components B_x, B_y and B_z of the local magnetic induction in the centre of the screened volume (at the intersection of the three axes). Here *x*, *y* and *z* are the axes of the triaxial structure (dashed lines in figure 3).

3. Results and discussion – uniaxial structure

3.1. First configuration

For the first configuration (figure 2(a)), the direction of the applied magnetic field is varied from the axial direction (θ = 0°) to the transverse direction (θ = 90°). The shielding performances are characterized by $B_{//}$, the component of the flux density which is parallel to the applied field H_{app}. The dimensionless parallel shielding factor $SF_{//}$ is defined as the ratio between $B_{app} = \mu_0 H_{app}$ and the parallel magnetic induction $B_{//}$. Both parameters are plotted in figure 4. As can be seen, the magnetic shielding is the most effective at θ = 0°, i.e. the axial configuration. When θ is increased from 0° to 90°, $B_{//}$ is still smaller than B_{app} but increases with both B_{app} and θ. For θ = 90°, i.e. for the transverse orientation, the parallel component of flux density $B_{//}$ is close to B_{app}, corresponding to a rather small field reduction (B_{app} - $B_{//}$ ≈ 1.1 mT).

This strong angular dependence is in contrast with magnetic shielding properties that can be obtained on bulk hollow tubes [10, 30]. In bulk samples, the shielding properties in transverse configuration (θ = 90°) are mainly due to currents flowing in the axial direction and closing near the tube opening ends ("saddle shape" currents). Such currents cannot flow from one tape to another in the present stack.

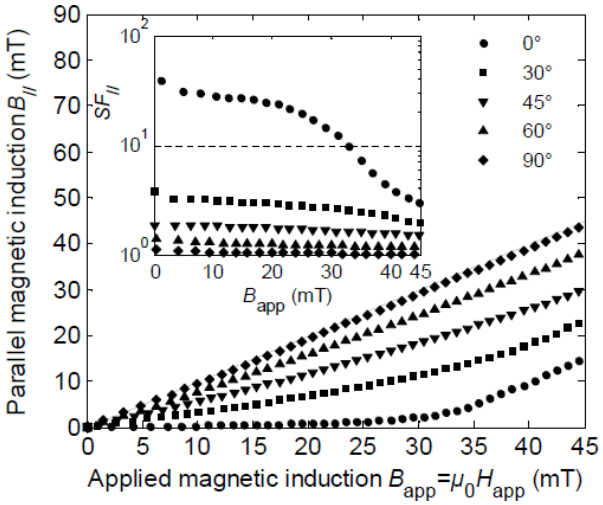

Figure 4. Parallel magnetic induction $B_{//}$ measured at the centre of the structure as a function of the applied magnetic induction B_{app} for θ = 0°, 30°, 45°, 60° and 90°. Inset: parallel shielding factor $SF_{//}$= B_{app}/ $B_{//}$ measured at the centre of the structure as a function of the applied magnetic induction B_{app}.

3.1.1 Magnetic flux density generated by the stack.

In order to understand in detail how the structure reacts to the applied magnetic field and which parameters affect the angular dependence of the shielding performances we first calculate the flux density $\mathbf{B}^{ind}$ induced by the shield, i.e. $\mathbf{B}^{ind} = \mathbf{B} - \mathbf{B}_{app.}$ Knowing $\mathbf{B}^{ind}$ we can calculate the angle δ between the vector of the applied magnetic induction $\mathbf{B}_{app}$ and $\mathbf{B}^{ind}$ from the scalar product $\mathbf{B}^{ind} \cdot \mathbf{B}_{app}$:

$$\delta = \arccos\left(\frac{\mathbf{B}^{ind} \cdot \mathbf{B}_{app}}{\|\mathbf{B}^{ind}\| \|\mathbf{B}_{app}\|}\right) \quad (1)$$

Figures 5 and 6 show respectively the modulus $\|\mathbf{B}^{ind}\|$ and the angle δ at the centre of the stack as a function of the applied magnetic induction B_{app}.

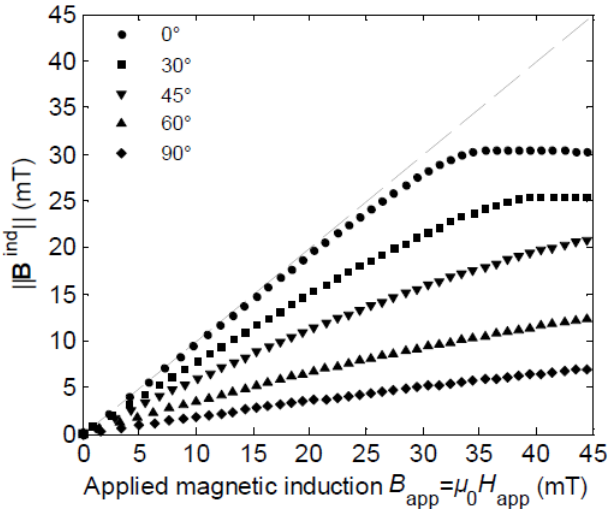

Figure 5. Modulus of the induced magnetic flux density $\|\mathbf{B}^{ind}\|$ at the centre of the stack as a function of the applied magnetic field $B_{app} = \mu_0 H_{app}$ for θ = 0°, 30°, 45°, 60° and 90°. The dashed line represents the $\|\mathbf{B}^{ind}\| = B_{app}$ line.

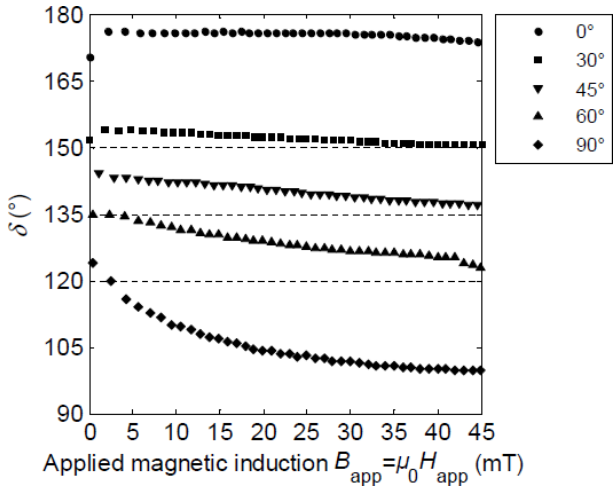

Figure 6. Angle δ between the vector $\mathbf{B}_{app}$ ($=\mu_0\mathbf{H}_{app}$) of the applied magnetic field and the vector $\mathbf{B}^{ind}$ of the magnetic flux density induced by the stack, as a function of the applied magnetic field $B_{app} = \mu_0 H_{app}$ for θ = 0°, 30°, 45°, 60° and 90°. The horizontal dashed lines are placed at (180° - θ) for the investigated θ.

Results plotted in figure 5 show that the modulus $\|\mathbf{B}^{ind}\|$ of the induced magnetic induction increases with the applied field, but decreases with θ. For B_{app} = 45 mT (i.e. the largest magnetic field that can be applied with the experimental set-up), the maximum and minimum values of $\|\mathbf{B}^{ind}\|$ are respectively 30 mT (at θ = 0°) and 7 mT (at θ = 90°). We note also that (i) the saturation is not observed for θ > 30° and that (ii) there is an induced magnetic induction for all values of θ. As can be seen in figure 6, the angle δ between $\mathbf{B}^{ind}$ and the applied magnetic induction $\mathbf{B}_{app}$ decreases with increasing θ and tends towards to (180°- θ) for θ = 0°, 30°, 45° and 60°. For θ = 90°, $\delta \approx$ 100° for B_{app} = 45 mT.

The angle δ and of the modulus $\|\mathbf{B}^{ind}\|$ allow us to identify some important features that are characteristic of magnetic field attenuation with the coated conductor structure. First, even in the axial direction (θ = 0°), the magnetic flux density induced by the stack is *not* completely anti-parallel to the applied field ($\delta \approx$ 175°). This property is likely to be due to the vertical offset between the two legs of each current loop. As a consequence, the average plane in which shielding currents flow is slightly tilted at some angle (hereafter called β) with respect to the plane normal to the *z*-axis. More precisely, if the structure has a radius *R* and is made of coated conductor sections of tape width w_{cc} and if the leg of the loop has a width w_l, β is approximately given by $\beta = \arctan\left((w_{cc} - w_l)/2R\right)$. In the present configuration, this gives β = 6.2°, which is quite close to the experimental (180° - $\delta \approx$

5°) value mentioned above. In principle, this shortcoming can be readily remedied in a shield consisting of two layers (an even number of layers to be precise), each similar to that in figure 1, but with oppositely offset relative to each other loops. Then the angle β defined above will be of the opposite side for the two layers and the misaligned components of the magnetic field will cancel each other out.

Second, results plotted in figures 4 and 5 show that in the transverse configuration ($\theta = 90°$), the field induced by the loop (e.g. 7 mT at the highest applied field) is much larger than the field attenuation that can be achieved in the direction of the applied field (1.1 mT in figure 4). This phenomenon is related to the fact that the induced field and the applied field are nearly orthogonal ($\delta \approx 100°$ on figure 6). This indicates clearly that the persistent currents in each stack generate a magnetic field that is nearly parallel to the *z*-axis of the stack. Therefore, the ability of the stack to shield the applied magnetic field decreases with θ because the magnetic field induced by the stack tends to be misaligned with respect to the direction of the applied magnetic field.

A further discussion of the distribution of the shielding currents in the tapes can be found in Appendix A. Using a simple model involving three kinds of possible current loops, we are able to explain (i) why there is an induced magnetic induction for all values of θ, (ii) why the induced magnetic induction decreases when θ increases and (iii) why the angle δ between the induced magnetic induction and the applied magnetic field decreases with θ.

3.2. Second configuration

In this section, our goal is to examine the performance of the shield in the applied DC field that lies in a plane perpendicular to the *z*-axis of the stack (figure 2(b)). The field is rotated in this plane with an angle α ranging from 0° to 90° with a 15° step. The angular position $\alpha = 0°$ corresponds to the $\theta = 90°$ case discussed in the previous section. Although the stack in this configuration provides only small field attenuation in the DC regime, we will show that several features of the angular dependence as a function of α can be explained qualitatively.

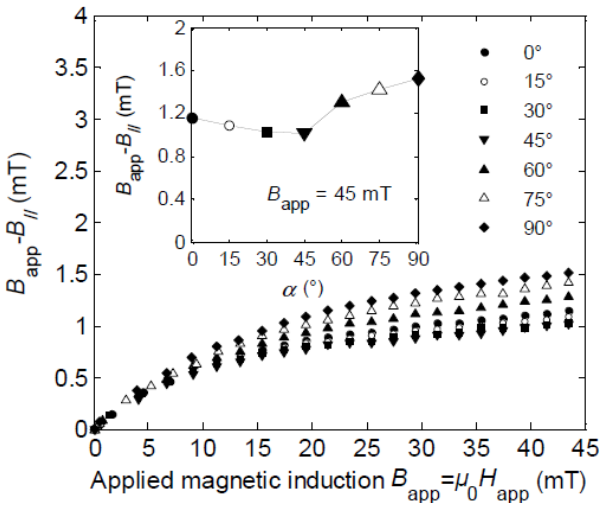

Figure 7. Difference B_{app}-$B_{//}$ as a function of the applied magnetic field $B_{app} = \mu_0 H_{app}$ for $\alpha = 0°$, 15° 30°, 45°, 60°, 75° and 90°. Small values of this quantity indicate weak screening of the external field by the shield.

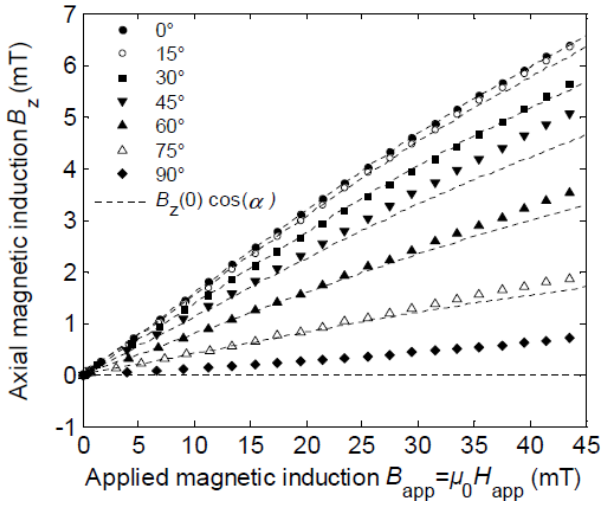

Figure 8. Measured axial component of the magnetic flux density B_z as a function of the applied magnetic field $\mu_0 H_{app}$ for α = 0°, 15° 30°, 45°, 60°, 75° and 90°. The dotted lines represent the approximation $B_z(\alpha) \approx B_z(0°)\cos(\alpha)$.

Figure 7 shows the difference B_{app} - $B_{//}$ between B_{app} (= $\mu_0 H_{app}$) and the parallel magnetic flux density $B_{//}$, as a function of the applied magnetic field. This difference, B_{app} - $B_{//}$, is quite small for all α angles ranging from 0° to 90°. However, the evolution of B_{app} - $B_{//}$ as a function of the angle α is not monotonous (inset to figure 7): it exhibits a small decrease (for α angles ranging from 0° to 45°), followed by an increase (for angles ranging from 60° to 90°). At the highest applied field (45 mT), the field reduction B_{app} - $B_{//} \approx$ 1.5 mT is the greatest for α = 90° and the smallest for α = 45°, where B_{app} - $B_{//} \approx$ 1 mT. The peculiar non-monotonic behaviour can be related to the eye-shape of superconducting current loops and is discussed in more details in Appendix B.

Figure 8 shows the axial component of the measured magnetic flux density at the centre of the structure as a function of the applied field. We recall here that the applied field is perpendicular to the axis of the structure, i.e. the axial component of the field in the absence of superconductor is strictly zero. The axial flux density values plotted in figure 8 are therefore due to supercurrents induced in the stacked loops. Figure 8 shows that the axial component increases with the applied field but decreases with α. Remarkably, the experimental curves measured for 0°< α < 90° can be estimated to a good approximation from the curve for α = 0° using the relation $B_z(\alpha) \approx B_z(0)\cos(\alpha)$. This approximation is the best at small applied fields and gives therefore a good estimation of the slope of B_z v.s. B_{app} at the origin.

The results plotted in figure 8 point out the principal property of coated conductors placed in this configuration: instead of magnetic shielding, they produce a modification of the direction of field at their centre. Such a field diversion is often desirable when the performances of a material or device are affected by the magnetic field direction. A typical example is the strong field-dependence of J_C of superconducting tapes of films with respect to the direction of the applied field. The two advantages of using stacks of tapes for diverting the field instead of conventional iron yoke are (i) the scalability to large volumes and (ii) their much lower weight.

The distribution of the shielding currents in this configuration is discussed in details in Appendix B and allows us to explain qualitatively the field dependence of the magnetic flux density in the direction of the applied magnetic field, the magnetic flux density parallel to the axis of the stack and the magnetic flux density induced by the superconductor.

4. Results and discussion – Triaxial structure

We now turn to the behaviour of the 3-axis screen described in section 2.2. We consider successively the magnetic shielding properties for 3 orientations of the applied field: (a) field parallel to one of the axes (b) field directed at 45° with respect to two axes, (c) field directed at the same angle with respect to the three axes.

4.1. First orientation

For the first orientation, the direction of the applied magnetic field is parallel to the *z*-axis (figure 3(a)).

Figure 9 shows applied field dependence of the local magnetic flux density components B_x, B_y and B_z (in the frame of the superconducting structure), as well as the modulus $\|\mathbf{B}_{in}\|$, measured at the centre of the structure, i.e. at the intersection of the three orthogonal axes.

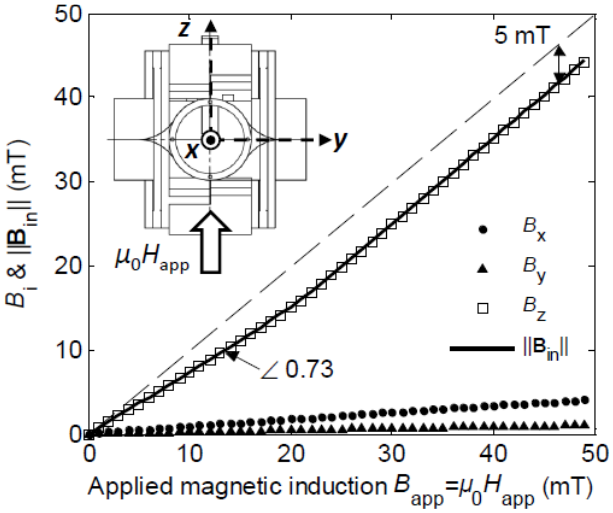

Figure 9. Local magnetic induction components B_x (●), B_y (▲) and B_z (□) as a function of the applied magnetic field $B_{app} = \mu_0 H_{app}$ for orientation (a). The plain line is the modulus $\|\mathbf{B}_{in}\| = \sqrt{B_x^2 + B_y^2 + B_z^2}$. The symbol "∠" shows the slope of the $\|\mathbf{B}_{in}\|$ vs. B_{app} curve at the origin. The dashed line represents the $\|\mathbf{B}_{in}\| = B_{app}$ line.

As can be seen on figure 9, the structure provides a small field reduction (defined as the difference B_{app} - $\|\mathbf{B}_{in}\|$) at the intersection of the three axes. For B_{app} > 25 mT, this field reduction is almost constant and equal to 5 mT. We can also observe the relatively large value of the dimensionless initial slope of $\|\mathbf{B}_{in}\|$ vs. B_{app} (0.73). This indicates that the structure is characterized by a fairly small shielding factor for low applied magnetic fields.

These features are due to the gap size between both stacks (6 cm) of the *z*-axis and by the small aspect ratios (0.09) of the individual stacks. Furthermore, we can see that components B_x and B_y are small with respect to B_z. As a consequence $\|\mathbf{B}_{in}\| \approx B_z$. Interestingly, however, B_x is found to be larger than B_y. This result can be understood easily from the results obtained in the previous section for the 1-axis structure. In the present configuration where the field is parallel to the *z*-axis, both pairs of coils with their axis parallel to *x* and *y* are subjected to a transverse field. In this configuration, the shielding currents induced in each loop produce a magnetic field directed along the axis of the coil, i.e. along *x* and *y*. Results plotted in figure 8, however, show that the orientation of the junction between the two legs of the loops (denoted by the angle α in the previous section) has a profound impact on the induced field. In the present case, the coil with its axis parallel to *x* corresponds to α = 0° and that with its axis parallel to *y* corresponds to α = 90°. As a consequence, the *x*-axis coil is more sensitive to the transverse magnetic field than the *y*-axis coil. Finally, since the coated conductor distribution is such that the average critical current density is the same in each of the three axes, we can expect similar results if the external magnetic induction is applied along *x* or *y* axis.

4.2. Second orientation

For the second orientation, the structure is rotated with respect to *x*-axis so that *y* and *z* axes make a 45° angle with respect to the direction of the applied magnetic field (figure 3(b)).

Figure 10 shows the applied field dependence of the local magnetic flux density components B_x, B_y and B_z, (in the frame of the superconducting structure), as well as the modulus $\|\mathbf{B}_{in}\|$ measured at the centre of the structure, i.e. at the intersection of the three orthogonal axes.

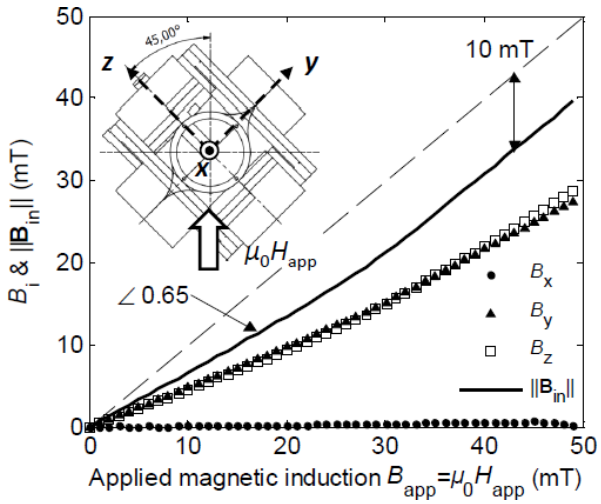

Figure 10. Local magnetic induction components B_x (●), B_y (▲) and B_z (□) as a function of the applied magnetic field $B_{app} = \mu_0 H_{app}$ for orientation (b). The plain line is the modulus $\|\mathbf{B}_{in}\| = \sqrt{B_x^2 + B_y^2 + B_z^2}$. The dashed line represents the $\|\mathbf{B}_{in}\| = B_{app}$ line.

As can be seen on figure 10, *y* and *z* axes have now nearly the same contribution as $B_y \approx B_z$ and, the component B_x measured in the *x*-axis, which remains orthogonal to the direction of the applied magnetic induction, is nearly zero. As a consequence: $\|\mathbf{B}_{in}\| \approx B_y\sqrt{2} \approx B_z\sqrt{2}$. The initial slope of $\|\mathbf{B}_{in}\|$ vs. B_{app} is around 0.65 and, for B_{app} > 30 mT, the slope is equal to 1. Finally, there is a field reduction of about 10 mT at the intersection of the three axes for B_{app} > 30 mT. These results will be discussed in section 4.4. below, together with those obtained for the third orientation.

4.3. Third orientation

For the third orientation, all three mutually orthogonal axes have the same orientation ($\arccos\left(1/\sqrt{3}\right) \approx 54.74°$) with respect to the direction of the applied magnetic field (figure 3(c)).

Figure 11 shows the magnetic flux density components B_x, B_y and B_z as well as the modulus $\|\mathbf{B}_{in}\|$ measured at the centre of the structure.

As can be seen on figure 11, all axes have the same contribution as $B_x \approx B_y \approx B_z$. As a consequence: $\|\mathbf{B}_{in}\| \approx B_x\sqrt{3} \approx B_y\sqrt{3} \approx B_z\sqrt{3}$. The initial slope of $\|\mathbf{B}_{in}\|$ vs. B_{app} is around 0.65 and, for B_{app} > 30 mT, the slope is equal to 1. Finally, there is a field reduction of about 10 mT at the intersection of the three axes for B_{app} > 30 mT.

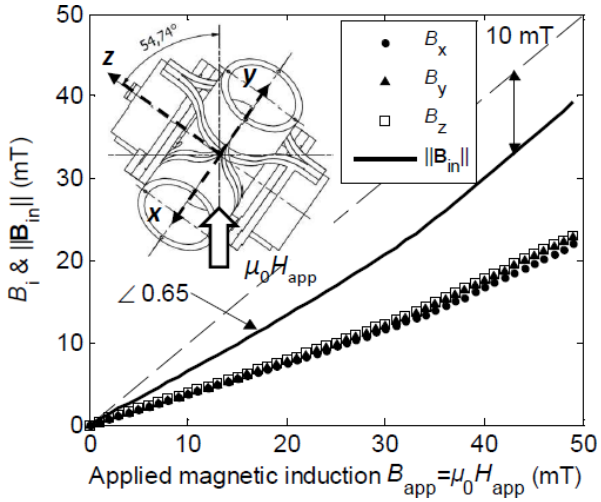

Figure 11. Local magnetic induction components B_x (●), B_y (▲) and B_z (□) as a function of the applied magnetic field $B_{app} = \mu_0 H_{app}$ for orientation (c). The plain line is the modulus $\|\mathbf{B}_{in}\| = \sqrt{B_x^2 + B_y^2 + B_z^2}$. The dashed line represents the $\|\mathbf{B}_{in}\| = B_{app}$ line.

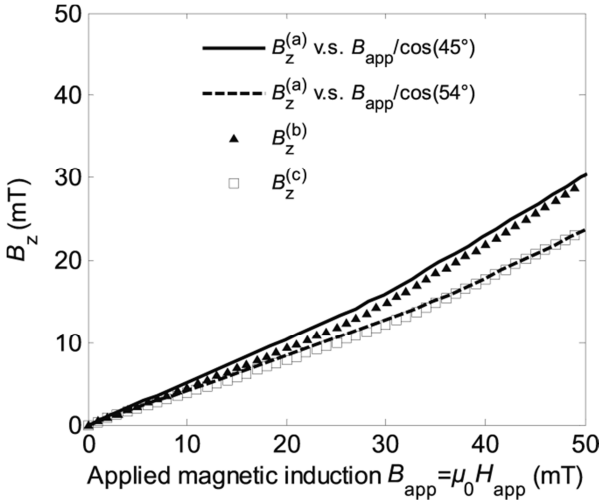

Figure 12. Approximation of the B_z component as a function of the applied magnetic induction B_{app} for orientations (b)(▲) and (c)(□) from the measurements of B_z in orientation (a).

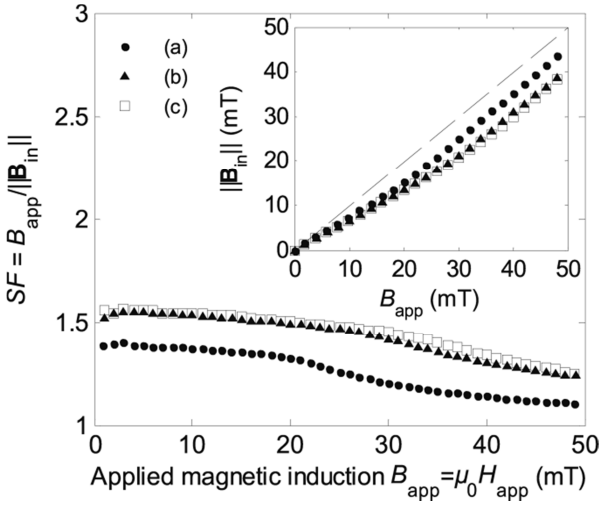

Figure 13. Shielding factor $SF = B_{app}/\|\mathbf{B}_{in}\|$ measured at the centre of the structure as a function of the applied magnetic field $B_{app} = \mu_0 H_{app}$ for orientations (a)(●), (b)(▲) and (c)(□). Inset: modulus of the magnetic induction $\|\mathbf{B}_{in}\|$ measured at the centre of the structure. The dashed line represents the $\|\mathbf{B}_{in}\| = B_{app}$ line.

4.4. Comparison between the three orientations

Figure 12 shows how the magnetic induction B_z for orientations (b) and (c) can be deduced from the measurement of B_z for orientation (a). This can be achieved by plotting $B_z^{(a)}$ as a function of $B_{app}/\cos(\gamma)$ with γ = 45° for orientation (b) and $\gamma = \arccos\left(1/\sqrt{3}\right) \approx 54°$ for orientation (c). For orientation (b), the approximation can be used to estimate the component B_y because the results have shown that $B_z \approx B_y$. For orientation (c), we can have estimation of B_x and B_y because the results have shown that $B_z \approx B_x \approx B_y$. It must be mentioned that the approximation does not account for the decrease of the axial magnetic induction with the angle between the axes and the applied magnetic field.

Figure 13 shows the applied field-dependence of the shielding factor $SF = B_{app}/\|\mathbf{B}_{in}\|$. The inset compares the modulus $\|\mathbf{B}_{in}\|$ at the centre of the structure for the three field orientations investigated.

This comparison emphasizes the fact orientations (b) and (c) give nearly identical results. Furthermore, the field attenuation for orientations (b) and (c) (about 10 mT) is twice larger than that of orientation (a) (about 5 mT). Results plotted in figure 13 show that orientations (b) and (c) have nearly the same shielding factor, corresponding to the inverse of their initial slope: 1/0.65 = 1.53. Furthermore, the shielding factor for B_{app} < 20 mT is found to be nearly constant and is increased by a factor 1.13 when the orientation increases from 0° to 45°, i.e. from orientation (a) to orientation (b).

The orientations (b) and (c) are found to give better results than orientation (a) because *z* axis and *y* axis (as well as *x* axis, in orientation (c)) contribute to the field reduction, i.e. their vectors of induced magnetic induction add up and the resultant vector is higher than that of orientation (a). Another reason is that, for orientation (a), the *x*-axis produces a magnetic induction that is perpendicular to the applied magnetic field (as evidence from results obtained in the uniaxial structure). As a result, the total magnetic induction generated by the structure is deviated and is not exactly parallel to the direction of the applied magnetic field.

Notwithstanding the additional contribution of the *x* axis in configuration (c), the similar results for orientations (b) and (c) can be explained as follows: for the orientation (c), the three axes contribute to the field reduction but the magnetic induction produced by the axes are smaller than that for orientation (b) because their angle with respect to the applied magnetic field is higher (54°) than that for the orientation (b) (45°).

In opposition to a 1-axis shield in a transverse orientation (section 3), the 3-axis structure gives a larger reduction of the applied magnetic field. If we consider each axis separately, the flux density induced by induced currents in each loop is not parallel to the direction of the applied magnetic field. If we consider the combination of two or three axes and if we assume that the different axes generate the same axial magnetic induction and that they have the same orientation with respect to the direction of the applied magnetic field, the resultant flux density induced by the structure is parallel to the direction of the applied magnetic field. As a result, the 3-axis structure is able to reduce a magnetic field that is not necessarily parallel to one axis of the structure. Finally, for the investigated orientations, the shielding factor of the 3-axis structure is nearly constant with the orientation whereas the shielding factor of a single axis shield decreases rapidly with the orientation.

4.5. Analytical prediction for orientation (a)

In previous results, on the graphs of $\|\mathbf{B}_{in}\|$ vs. B_{app} for the three orientations, we can observe that the curve of $\|\mathbf{B}_{in}\|$ vs. B_{app} displays two parts, as shown schematically on figure 14. Part *I* is nearly linear

and the slope *s* of $\|\mathbf{B}_{in}\|$ vs. B_{app} at the origin depends only slightly on the magnetic field orientation. Part *II* is nearly linear with a slope equal to 1, so that the field reduction B_{app} - $\|\mathbf{B}_{in}\|$ is independent of B_{app}, and is a function of the orientation. We have shown in our earlier work [26] that part *II* is also a function of the number of layers, and therefore function of J_C. As a consequence, the second part will be shifted to the right when J_C (or I_C) increases. Figure 14 shows the approximation of $\|\mathbf{B}_{in}\|$ as a function of B_{app}.

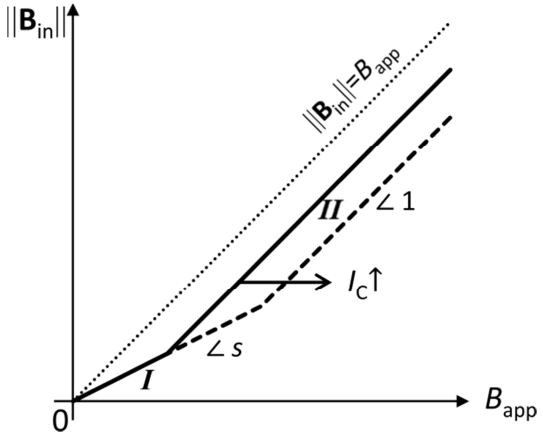

Figure 14. Schematic illustration of the magnetic induction $\|\mathbf{B}_{in}\|$ as a function of the applied magnetic field $B_{app} = \mu_0 H_{app}$. The plain line represents the $\|\mathbf{B}_{in}\|$ v.s. B_{app} behaviour in a given configuration and the dashed lines shows how the results are modified if the critical current of the tapes is increased.

The aim of this section is to predict analytically the field reduction B_{app} - $\|\mathbf{B}_{in}\|$. The configuration investigated is that for which the external magnetic field is applied along one axis of the structure, since experimental results above have shown clearly that the field reduction is always larger when the applied field is applied at some angle with respect to one of the axes. According to experimental results obtained for the orientation (a) (figure 9), we will further assume that the contribution of the two orthogonal axes can be neglected, in such a way that $\|\mathbf{B}_{in}\| = B_z$.

Knowing the individual critical currents of each coated conductor sections (obtained by measuring their trapped field [26, 29]), we can have a good estimation of the axial component of the trapped field or of the field B_z^{ind} induced by the stack. As this value is approximately the difference B_{app} - B_z, we can estimate the field reduction at the centre of the structure.

The approximation consists in assuming each stack of the *z*-axis as a coil of circular cross section. The critical current is assumed to be the same for each coated conductor section so that the current flowing in the coils is I_C. Table 3 gives the geometrical parameters of the structure.

Table 3. Geometric parameters.

Number of loops stacked along the axis	N
Number of layers (superimposed tapes)	m
Total number of loops	$N.m$
Radius of the supporting cylinder and of a loop	R
Distance between the mid-plane of the loops[a,b]	$z_s = (w_{cc}\text{-}w_{cut})/2$
Height of a stack	$h = (N/2\text{-}1)\, z_s$
Gap between two stacks on the same axis	$2d = 2R + w_{cc}$
Total height of an axis	$h_{tot} = 2(d+h)$

[a] w_{cc} = 12 mm is the width of a superconducting tape.
[b] w_{cut} = 1 mm is the width of the cut.

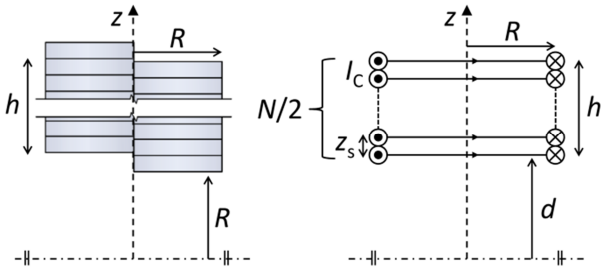

Figure 15. Geometrical parameters and approximations of a stack made of *N*/2 current loops.

The magnetic flux density at the centre of the structure induced by shielding currents can be obtained from the analytical expression of the magnetic induction along the axis of a coil (Biot-Savart law) [31]:

$$B_z^{\text{ind}}(z=0)=\frac{\mu_0 N m I_C}{2h}\left[\frac{h+d}{\sqrt{(h+d)^2+R^2}}-\frac{d}{\sqrt{d^2+R^2}}\right] \tag{2}$$

where

$$h = (N/2\text{-}1)\, z_s \tag{3}$$

From this expression, we can see that, for a given geometry (i.e. fixed radius *R* and gap *d*) and a given current I_C, the induced induction can be increased by increasing *N* and/or *m*. For $m.I_C$ =250 A (typical value used in the experiment (cf. table 2)), *N* = 4 and *R* = 30 mm we found B_z^{ind} = 4.8 mT which is remarkably close to the 5 mT attenuation found in the experiment. Therefore one can conclude that this analytical model, although very simple, is able to predict the DC magnetic field attenuation of a 3-axis structure of any size, configuration and coated conductor properties. This will be investigated in the last section below.

4.6. Improvement of performances for orientation (a)

In the previous sections, the relatively small DC field attenuation was explained by the gap size between axes stacks and by their low aspect ratio. Clearly, the gap between axis stacks is unavoidable, unless reducing the diameter of the supporting cylinder. The low aspect ratio of the stack was due to practical considerations, i.e. the number of tapes available for the experiment. If the size of the structure is not a problem, performances could be possibly improved by changing the geometrical parameters of the stacks, i.e. by increasing the aspect ratio (which means increasing the number of coated conductor sections along the axis) and/or by increasing the number of layers. We have shown in [26] that the shielding factor at the centre of the shield increases with the aspect ratio and that the threshold induction increases with the aspect ratio and the number of layers. However, the performances at extremities of the shield are always reduced by the penetration through the open end of the structure and so slightly increase with the aspect ratio.

Using the simple analytical model developed in the previous section (figure 15), we can now estimate the value of magnetic flux density at the centre of the stack that could be expected when the number of coated conductor sections is changed. For a high number of turns *N*, the induced magnetic flux density at the centre of the structure will reach an asymptotic value given by:

$$B_z^{\text{ind}}(z=0)\rightarrow\frac{\mu_0 m I_C}{z_s}\left(1-\frac{d}{\sqrt{d^2+R^2}}\right) \tag{4}$$

The physical explanation is that when *N* increases, the effect of the most distant loops on B_z^{ind} at *z* = 0 decreases.

For I_C =125 A and a single layer (*m* = 1), the induced magnetic flux density at the centre would be 6.6 mT. This value is reached for approximately 100 coated conductors (50 for each stack) and the total

height of the structure h_{tot} is 61.1 cm. As a conclusion, adding more tapes along the axis of the structure is clearly not the best way of improving magnetic shielding. To increase the field attenuation, it is more convenient to increase the number of superimposed layers. As the maximum magnetic induction is proportional to I_C, if the stacks contain m layers, the total current will be multiplied by m as well as the maximum magnetic induction. For example, for I_C =125 A, N = 4 and m = 3, B_z^{ind} = 7.2 mT which is higher than the field obtained with a single layer and N = 100.

5. Conclusion

We have investigated the DC magnetic behaviour of 1-axis and 3-axis structures made of stacks of short-circuited coated conductors. We have first examined the properties of the 1-axis structure when the applied field is not parallel to the axis of the stack. Because of the absence of symmetry of revolution of the assembly, two configurations for the orientation of the applied magnetic field with respect to the assembly were studied. In the first configuration, the direction of applied magnetic field is varied from the axial direction (θ = 0°) to the transverse direction (θ = 90°). The direction of the applied magnetic field remains parallel to the plane of symmetry *yz*. For the second configuration, the main *z*-axis of the shield remains perpendicular to the direction of the applied magnetic field and the stack is rotated around its main *z*-axis with an angle α ranging from 0° to 90°.

In the first configuration, results have shown that the shielding efficiency is maximum when the magnetic field is applied along the axis of the shield and that the performances decrease rapidly when the angle θ is increased. Furthermore, the most significant result is the determination of the total magnetic flux density $\mathbf{B}^{ind}$ generated by these induced current loops and its angle δ with respect to the applied field. We have shown that the stack reacts to the applied magnetic field for all values of θ, i.e. that the applied magnetic field generates supercurrents in the tapes. However, supercurrents generate a magnetic induction whose the orientation remains nearly parallel to the *z*-axis of the stack for all values of θ, and whose amplitude decreases with θ.

Next we have examined in details the second configuration in which the field is rotated at some angle α within the plane perpendicular to the axis. In this case, the applied field generates supercurrents in the loop, but the magnetic field induced by these currents has again a large component along the *z*-axis of the stack (for α < 45°). For α > 45° the induced magnetic induction becomes progressively antiparallel to the direction of the applied magnetic field but we observed that its amplitude decreases for all values of α. As a consequence, the field attenuation in the direction of the applied field is very small for all values of α. The magnetic properties are found to depend significantly on α, and this feature is linked to the eye-shape of each loop of the stack. The angular dependence can be explained by the particular eyed-shape of the coated conductor sections and by the possible contributions of the induced current loops to the resulting flux density at the centre of the stack. Instead of magnetic shielding, coated conductors placed in this configuration produce thus a modification of the direction of field at their centre.

Such a modification of the direction of a DC field can therefore be achieved using one of several loops of coated conductors placed around the zone of interest. The comprehensive set of results obtained in this work for various angular positions (θ and α) of the applied field with respect to the loop allow the direction of the resulting DC flux density ($\mathbf{B} = \mathbf{B}_{app} + \mathbf{B}^{ind}$) to be predicted. The interest of modifying the direction of the applied field can be used in applications where the performances are affected by the magnetic field direction, e.g. the strong field-dependence of J_C of superconducting tapes of films with respect to the direction of the applied field. The advantages of using stacks of tapes instead of conventional iron yoke are the scalability and their much lower weight.

The results obtained for the 1-axis structure point out that the DC magnetic properties of a stack of coated conductor sections in the transverse configuration differ considerably from those obtained with a HTS hollow cylinder subjected to a transverse magnetic field [10, 32]. The main difference with HTS hollow cylinders in transverse configuration is the absence of large saddle-shaped shielding currents loops.

In the second part of the work, the field attenuation of a structure made of three orthogonal axes was studied for three orientations of the applied magnetic field, i.e. (i) along one axis of the structure, (ii) at 45° with respect to two axes, and (iii) at the same orientation with respect to the three mutually orthogonal axes. Results show that the structure is able to provide a moderate reduction of the applied magnetic field, the corresponding shielding factor being lower than 10 for all orientations. The field reduction and the shielding factor are minimum when the field is applied along one axis and they increase when the orientation is increased from 0° to 45° because the magnetic flux densities generated by the two axes add up. The results for the second (45°) and the third (54°) orientations are very similar, this feature results from the angular dependence of the magnetic behaviour of individual axes. The modest performances are explained by the gap size between both stacks (6 cm) of each axis and, by the small aspect ratios (0.09) of the individual stacks. The 3-axis structure, however, gives better results than that obtained for the uniaxial structure in transverse orientation because of the contributions of the two other axes. Finally, a simple analytical model has been used to predict the possible improvement of the performances of such a structure. Results show that adding of more layers is much more efficient than stacking additional coated conductors along the orthogonal axes.

Acknowledgements

The authors thank the Royal Military Academy for the YBCO tapes and, FNRS and the University of Liège for cryofluid, equipment and travel grants.

Appendix A. Discussion about the first configuration of the uniaxial structure

To understand further the experimental facts discussed in section 3.1, we first consider a single loop of the stack, represented in figure A1. In the coordinate system *xyz* associated with the loop, the applied magnetic induction has an axial component $B_{app}\cos(\theta)$ and a transverse component $B_{app}\sin(\theta)$.

If we assume, in the first approximation, that the loop is a perfect ring, it would respond only to the axial component of the applied magnetic field. The variation of the axial component induces a superconducting current I_1 flowing through the loop, as shown in figure A1(b). However, because of the fabrication process, the two half parts of the loop lay in two different planes on either side of the *xy*-plane, as shown in figure A1(a). As a consequence, such a loop is also sensitive to the transverse component of the applied magnetic field. This transverse component induces two types of currents. First, a current I_2 is circulating in the entire loop because it is induced by the finite magnetic flux enclosed inside the loop. Note that in a loop in the form of a perfect band the transverse component of the applied field would not generate the persistent current. Second, because of the finite width of the half parts of the loop (5.5 mm in this case), localized shielding currents I_3 are also induced by the transverse applied magnetic field. The presence of such currents I_3 will affect the distribution of the total current in the cross section of each half part of the loop. The distributions of currents I_2 and I_3 are sketched in figure A1(b).

The currents I_1 and I_2 flowing in the entire loop generate a magnetic field along the *z*-axis of the loop and a much smaller magnetic field along *y*-axis. The contribution of current I_1 and I_2 on the component along *y*-axis is due to the tilt of the average plane in which shielding currents flow. This tilt is measured by the angle β (defined in section 3.1.1) with respect to the plane normal to the *z*-axis.

For $\theta = 0°$, the magnetic field induced by the persistent current circulating in the stack is at maximum because the magnetic flux of the external field through the area of the eye-shaped loop is maximal. On the contrary, for $\theta = 90°$, the magnetic field induced by the stack is at minimum because the external magnetic flux that the shield must screen out is minimal. Furthermore, the small field attenuation observed for $\theta = 90°$ can be attributed to the circulation of currents I_2 and I_3. This explains the results shown in figure 5. Note that the saturation of $\|\mathbf{B}^{ind}\|$ in figure 5 indicates that the persistent current has reached its maximum value and cannot be increased in response to the increasing external magnetic flux.

In the shield made out of several stacked loops, the magnetic induction generated along *z*-axis of the stack increases because the contributions from all the loops add up. In comparison to currents I_1 and I_2, the localized currents I_3 have a small contribution to the magnetic flux density at the centre of the loop because they are not flowing in the entire loop. In fact, currents I_3 are similar to those observed for hollow cylinders in transverse field configuration but the main difference is that, because the shield is made individual tapes, the area enclosed by these currents is much smaller than for a bulk material. As a result, the field attenuation provided by these currents is smaller than that obtained for a hollow cylinder. Note, that the screening of the transverse field by this type of shield can be improved by using wider coated conductors, like the 40 mm wide conductors used in [33, 34].

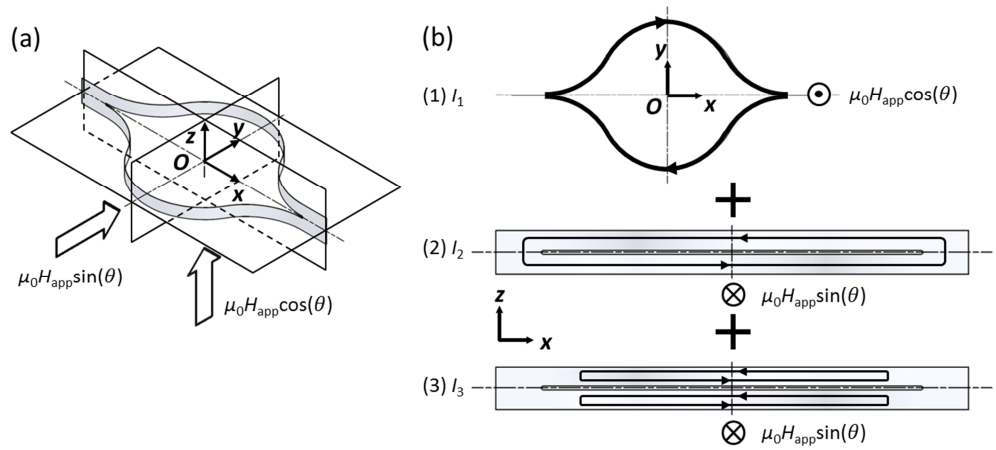

Figure A1. (a) Schematic view of a single loop. (b) Types of currents induced in a single loop by the axial and the transverse applied magnetic field.

Appendix B. Discussion about the second configuration of the uniaxial structure

B.1. Discussion: distribution of the shielding currents

In order to understand how the stack reacts to a magnetic field applied perpendicular to its axis and rotated in this plane, we consider a single loop of the stack (figure B1(a)). The applied magnetic induction B_{app}, applied in the *xy*-plane of the loop, can be separated in two components: $B_{app}\cos(\alpha)$, the component of B_{app} along the *y*-axis of the loop, and $B_{app}\sin(\alpha)$, the component of B_{app} along the *x*-axis of the loop (figure 2(b)). Because of the particular geometry of the loop, the component $B_{app}\cos(\alpha)$ injects a finite magnetic flux into the closed superconducting loops which, by virtue of magnetic flux conservation, induces the persistent current I_2 in the entire loop which tends to cancel the applied magnetic flux. Also are induced localized currents I_3 in both half parts of the loop, as shown schematically in figure B1(b). The component $B_{app}\sin(\alpha)$ does not introduce the magnetic flux into the closed loops and, therefore, it only induces the localized currents I_4 in both half parts of the loop, as shown in figure B1(b).

In the centre of the loop, at point *O*, the current I_2 circulating through the entire loop generates a magnetic flux density B_z^{ind} along *z*-axis of the loop and a smaller component of the flux density along the *y*-axis. When several loops are stacked together, the individual B_z^{ind} components add up.

The localized currents I_3 generate a resultant flux density along the *y*-axis and in two planes parallel on either side of the *xy*-plane. The localized currents I_4 generate a resultant magnetic induction along the *x*-axis and in two planes parallel on either side of the *xy*-plane. When several loops are stacked together, one half part of the loop and a half part the adjacent loop are facing each other so the magnetic inductions generated by localized currents I_3 and I_4 of both loops add up. In the two paragraphs below, we examine how this simple picture shown in figure B1 is able to explain the experimental results shown in figures 7-8 and in figures B2-B3.

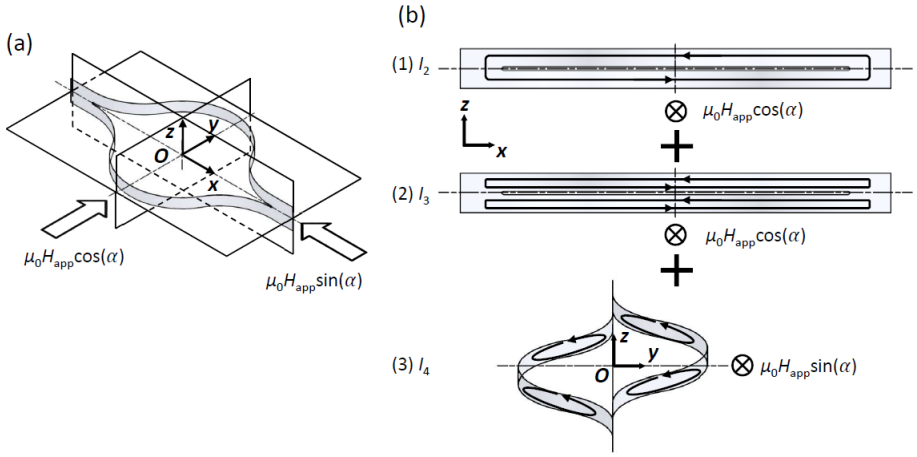

Figure B1. (a) Schematic view of a single loop subjected to a magnetic field applied in the *xy*-plane. (b) Schematic view of the current distribution in the loop.

B.2. Evolution of the magnetic flux density in the direction of the applied magnetic field

The difference (B_{app}-$B_{//}$) is the component of the induced magnetic induction $\mathbf{B}^{ind}$ that is parallel to the applied magnetic field (equation B1). It can be expressed as a function of both components B_x^{ind} and B_y^{ind} of the magnetic induction generated in the frame related to the stack:

$$B_{app} - B_{//} = B_x^{ind} \sin(\alpha) - B_y^{ind} \cos(\alpha) \quad (B.1)$$

We assume that B_x^{ind} is related to local currents I_4 and that B_y^{ind} is related to the current I_2 and to local currents I_3. We can also make the assumption that, for $\alpha = 0°$, $B_x^{ind}(\alpha = 0°) = 0$ (by symmetry with respect to *yz*-plane) and that $B_y^{ind}(\alpha = 0°)$ is maximum. For $\alpha = 90°$, we can assume that $B_x^{ind}(\alpha = 90°)$ is maximum and that $B_y^{ind}(\alpha = 90°) = 0$. For α angles ranging from 0° to 90°, the currents I_3 decrease so B_y^{ind} decreases but the currents I_4 increases so B_x^{ind} increases. For $\alpha = 0°$, the field is applied along the *y*-axis of the loop and the field reduction is provided by the shielding currents I_2 and I_3. Consequently $B_{app} - B_{//} = -B_y^{ind}$. For $\alpha = 90°$, the field is applied along the *x*-axis of the loop and the field reduction is provided by the shielding currents I_4. Consequently $B_{app} - B_{//} = B_x^{ind}$. For $0° < \alpha < 45°$, the evolution of $B_{app} - B_{//}$ is mainly determined by $B_y^{ind} \cos(\alpha)$ which decreases with α. As a result, $B_{app} - B_{//}$ decreases with α. For $45° < \alpha < 90°$, the evolution of $B_{app} - B_{//}$ is mainly determined by $B_x^{ind} \sin(\alpha)$ which increases with α. As a result, $B_{app} - B_{//}$ increases with α. This explains therefore the peculiar non-monotonic behaviour observed experimentally (inset of figure 7).

B.3. Evolution of the magnetic flux density parallel to the axis of the stack

The axial magnetic induction B_z^{ind}, which is equal to the measured axial magnetic induction, is generated by the current I_2 flowing in the entire loop. This current is found experimentally to depend on the component $B_{app}\cos(\alpha)$ of the applied magnetic field and decreases with α. Therefore, we can easily understand why the axial component B_z is maximum for $\alpha = 0°$ and minimum for $\alpha = 90°$. Theoretically, we should have B_z ($\alpha = 90°$) = 0. However, we observed $B_z \approx 0.75$ mT for $B_{app} = 45$ mT because (i) the *z*-axis of the stack was not perfectly perpendicular to the direction of the applied magnetic field and (ii) because the α angle itself was maybe not exactly equal to 90°.

B.4. Evolution of the induced magnetic flux density and of the δ angle

In a similar way to what was done in the first configuration, it is instructive to determine the amplitude and angle of the magnetic flux density induced by the stack. Figure B2 shows the modulus $\|\mathbf{B}^{ind}\|$ of the induced magnetic flux density at the centre of the stack as a function of the applied field. This modulus $\|\mathbf{B}^{ind}\|$ is found to increase with applied field but decreases with α. It is of interest to note that the *largest* field attenuation in the direction of the applied field, observed for $\alpha = 90°$ in figure 7, correspond to the *smallest* values of the magnetic flux density induced by the stack, as shown in figure B2.

Figure B3 shows the applied field dependence of the angle δ between the induced flux density and the applied field for several values of α. At the highest applied field, this angle δ is shown to be close to 100° for α ranging between 0° and 45°. For α > 45°, the angle δ increases with α and is maximum for α = 90°. This indicates that the direction of the induced magnetic flux density tends to become anti-parallel with that of the applied magnetic field. The α-dependence appearing in figure B3 is due to the particular eye-structure of the loops and is discussed as follows.

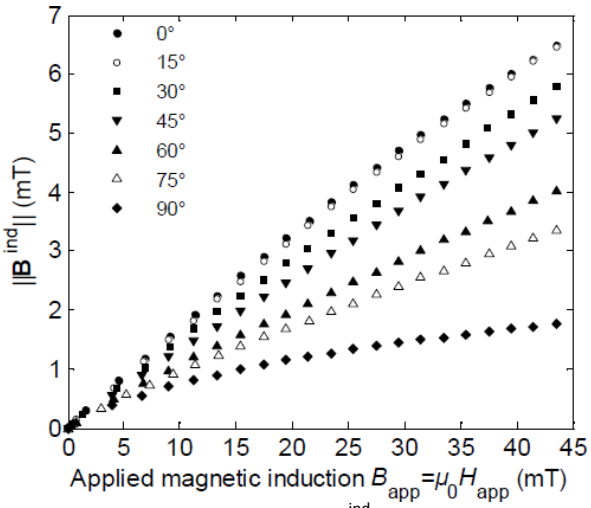

Figure B2. Modulus of the induced magnetic flux density $\|\mathbf{B}^{ind}\|$ at the centre of the stack as a function of the applied magnetic field $B_{app} = \mu_0 H_{app}$ for α = 0°, 15° 30°, 45°, 60°, 75° and 90°.

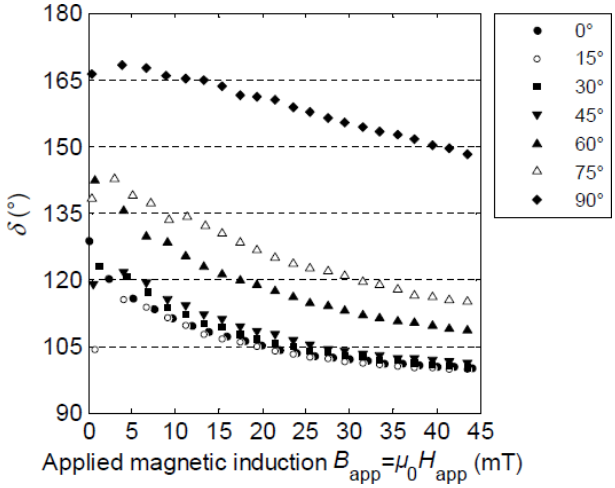

Figure B3. Angle δ between the vector $\mathbf{B}_{app} = \mu_0\mathbf{H}_{app}$ (applied magnetic field) and the vector $\mathbf{B}^{ind}$ of the magnetic flux density induced by the stack, measured at the centre of the structure as a function of the applied magnetic field $B_{app} = \mu_0 H_{app}$ for α = 0°, 15° 30°, 45°, 60°, 75° and 90°.

In the frame related to the stack, the modulus of the induced magnetic induction is:

$$\left\|\mathbf{B}^{ind}\right\| = \sqrt{(B_x^{ind})^2 + (B_y^{ind})^2 + (B_z^{ind})^2} \qquad (B.2)$$

For α = 0°, the axial magnetic induction B_z^{ind} is maximum and a small field reduction is provided by B_y^{ind}. As a result, the stack generates a magnetic induction $\mathbf{B}^{ind}$ that is mainly oriented along the axis of the stack because $B_z^{ind} > B_y^{ind} > B_x^{ind}$ and that is maximum because B_z^{ind} is maximum. This also explains why the angle δ between the applied magnetic field and the induced magnetic induction at the centre of the stack is close to 100° at the largest applied field (B_{app} = 45 mT).

For α angles ranging from 0° to 90°, B_z^{ind} and B_y^{ind} both decrease with α whereas B_x^{ind} increases with α. As a result, the induced magnetic induction decreases with α. For α angles ranging from 0° to 45° and for B_{app} = 45 mT, the angle δ remains close to 100° because $B_{app} - B_{//}$ and $\|\mathbf{B}^{ind}\|$ both decrease. For α angles ranging from 60° to 90° and for B_{app} = 45 mT, the angle δ increases because $B_{app} - B_{//}$

increases and $\|\mathbf{B}^{ind}\|$ decreases. For $\alpha = 90°$, the modulus $\|\mathbf{B}^{ind}\|$ is minimum because B_z^{ind} and B_y^{ind} are minimum.

References

[1] Giunchi G, Bassani E, Cavallin T, Bancone N and Pavese F 2007 An MgB2 superconducting shield for a cryogenic current comparator working up to 34 K *Superconductor Science and Technology* **20** L39-L41

[2] Arpaia P, Ballarino A, Giunchi G and Montenero G 2014 MgB2 cylindrical superconducting shielding for cryogenic measurement applications: a case study on DC current transformers *Journal of Instrumentation* **9** P04020

[3] Kamiya K, Warner B A and DiPirro M J 2001 Magnetic shielding for sensitive detectors *Cryogenics* **41** 401

[4] Kamiya K, Warner B A, DiPirro M J and Numazawa T 2003 Passive magnetic shielding for the submillimeter and far infrared experiment *Physica B: Condensed Matter* **329-333** 1627-8

[5] Lvovsky Y, Stautner E W and Zhang T 2013 Novel technologies and configurations of superconducting magnets for MRI *Superconductor Science and Technology* **26** 093001

[6] Prouvé T, Duval J M, Luchier N and D'escrivan S 2014 Experimental results on MgB2 used as ADR magnetic shields, and comparison to NbTi *Cryogenics* **64** 201-6

[7] Muething K A, Edwards D O, Feder J D, Gully W J and Scholz H N 1982 Small solenoid with a superconducting shield for nuclear-magnetic-resonance near 1 mK *Review of Scientific Instruments* **53** 485-90

[8] Burt E A and Ekstrom C R 2002 Optimal three-layer cylindrical magnetic shield sets for scientific applications *Review of Scientific Instruments* **73** 2699

[9] Fagnard J F 2011 Experimental and numerical study of the factors influencing the performances of magnetic screens made of high temperature superconductors. (Liège: University of Liège)

[10] Fagnard J F, Dirickx M, Ausloos M, Lousberg G, Vanderheyden B and Vanderbemden P 2009 Magnetic shielding properties of high-Tc superconducting hollow cylinders: model combining experimental data for axial and transverse magnetic field configurations *Superconductor Science and Technology* **22** 105002

[11] Fagnard J F, Elschner S, Bock J, Dirickx M, Vanderheyden B and Vanderbemden P 2010 Shielding efficiency and E(J) characteristics measured on large melt cast Bi-2212 hollow cylinders in axial magnetic fields *Superconductor Science and Technology* **23** 095012

[12] Matsuba H, Yahara A and Irisawa D 1992 Magnetic shielding properties of HTc superconductor *Superconductor Science and Technology* **5** S432

[13] Willis J, McHenry M E, Maley M P and Sheinberg H 1989 Magnetic shielding by superconducting Y-Ba-Cu-O hollow cylinders *IEEE Trans. Magn.* **25** 2502

[14] Closset R, Kumar N D, Wera L, Dellicour A, Henrist C, Boschini F, Cloots R, Vanderbemden P and Vertruyen B 2014 YBa2Cu3O7−δ thick films for magnetic shielding: Electrophoretic deposition from butanol-based suspension *Materials Letters* **119** 154

[15] Gozzelino L, Minetti B, Gerbaldo R, Ghigo G, Laviano F, Agostino A and Mezzetti E 2011 Local Magnetic Investigations of MgB2 Bulk Samples for Magnetic Shielding Applications *IEEE Trans. Appl. Supercond.* **21** 3146

[16] Cavallin T, Quarantiello R, Matrone A and Giunchi G 2006 Magnetic shielding of MgB2 tubes in applied DC and AC field *Journal of Physics: Conference Series* **43** 1015

[17] Lousberg G, Fagnard J F, Ausloos M, Vanderbemden P and Vanderheyden B 2010 Numerical Study of the Shielding Properties of Macroscopic Hybrid Ferromagnetic/Superconductor Hollow Cylinders *IEEE Trans. Appl. Supercond.* **10** 33-41

[18] Gozzelino L, Gerbaldo R, Ghigo G, Laviano F, Agostino A, Bonometti E, Chiampi M, Manzin A and Zilberti L 2013 DC Shielding Properties of Coaxial MgB2/Fe Cups *IEEE Trans. Appl. Supercond.* **23** 8201305

[19] Tomków Ł, Ciszek M and Chorowski M 2015 Combined magnetic screen made of Bi-2223 bulk cylinder and YBCO tape rings—Modeling and experiments *Journal of Applied Physics* **117** 043901

[20] Yuan W, Campbell A M and Coombs T A 2010 Design and modelling of a SMES coil *Journal of Physics: Conference Series* **234** 032068

[21] Senatore C, Alessandrini M, Lucarelli A, Tediosi R, Uglietti D and Iwasa Y 2014 Progresses and challenges in the development of high-field solenoidal magnets based on RE123 coated conductors *Superconductor Science and Technology* **27** 103001

[22] Kosa J, Vajda I and Gyore A 2010 Application possibilities with continuous YBCO loops made of HTS wire *Journal of Physics: Conference Series* **234** 032030

[23] Hong Z, Jin Z, Ainslie M, Sheng J, Yuan W and Coombs T A 2011 Numerical Analysis of the Current and Voltage Sharing Issues for Resistive Fault Current Limiter Using YBCO Coated Conductors *IEEE Trans. Appl. Supercond.* **21** 1198

[24] Kosa J, Vajda I and Kovacs L 2011 Novel Self-Limiting Transformer With Active Magnetic Short Circuit Using Perfect YBCO Wire Loops *IEEE Trans. Appl. Supercond.* **21** 1417-21

[25] Fagnard J F, Dirickx M, Levin G A, Barnes P N, Vanderheyden B and Vanderbemden P 2010 Use of second generation coated conductors for efficient shielding of dc magnetic fields *Journal of Applied Physics* **108** 013910

[26] Wéra L, Fagnard J-F, Levin G A, Vanderheyden B and Vanderbemden P 2013 Magnetic Shielding With YBCO Coated Conductors: Influence of the Geometry on Its Performances *IEEE Trans. Appl. Supercond.* **23** 8200504

[27] Kvitkovic J, Pamidi S and Voccio J 2009 Shielding AC magnetic fields using commercial YBa2Cu3O7-coated conductor tapes *Superconductor Science and Technology* **22** 125009

[28] Park J, Krall N A, Sieck P E, Offermann D T, Skillicorn M, Sanchez A, Davis K, Alderson E and Lapenta G 2014 High Energy Electron Confinement in a Magnetic Cusp Configuration **arXiv:1406.0133**

[29] Levin G A, Barnes P N, Murphy J, Brunke L, Long J D, Horwath J and Turgut Z 2008 Persistent current in coils made out of second generation high temperature superconductor wire *Applied Physics Letters* **93** 062504

[30] Mawatari Y 2011 Superconducting tubular wires in transverse magnetic fields *Physical Review B* **83** 134512

[31] Durand E 1968 *Magnétostatique* (Paris: Masson)

[32] Fagnard J F, Elschner S, Hobl A, Bock J, Vanderheyden B and Vanderbemden P 2012 Magnetic shielding properties of a superconducting hollow cylinder containing slits: modelling and experiment *Superconductor Science and Technology* **25** 104006

[33] Kvitkovic J, Davis D, Zhang M and Pamidi S 2013 Influence of Interlayer Separation on Magnetic Shielding Properties of 2G HTS Sheets Made of 46 mm Wide RABiTS Tape *IEEE Trans. Appl. Supercond.* **23** 8200605

[34] Kvitkovic J, Davis D, Zhang M and Pamidi S 2015 Magnetic Shielding Characteristics of Second Generation High Temperature Superconductors at Variable Temperatures Obtained by Cryogenic Helium Gas Circulation *IEEE Trans. Appl. Supercond.* **25** 8800304